AGU PUBLICATIONS

JGR

Journal of Geophysical Research: Space Physics

RESEARCH ARTICLE
10.1002/2014JA019994

Key Points:
- A plume of energetic (>2 keV) planetary ions is escaping from Mars
- The plume is directed along the solar wind motional electric field
- Clarity of plume signatures greatly depends on selected survey methodology

Supporting Information:
- Readme
- Figure S1
- Figure S2
- Figure S3
- Figure S4
- Figure S5
- Figure S6
- Figure S7
- Figure S8
- Figure S9
- Figure S10
- Figure S11
- Figure S12
- Figure S13
- Figure S14
- Figure S15
- Figure S16
- Figure S17
- Figure S18
- Figure S19
- Figure S20
- Figure S21
- Figure S22
- Figure S23
- Figure S24
- Figure S25
- Figure S26
- Figure S27

Correspondence to:
M. W. Liemohn,
liemohn@umich.edu

Citation:
Liemohn, M. W., B. C. Johnson, M. Fränz, and S. Barabash (2014), Mars Express observations of high altitude planetary ion beams and their relation to the "energetic plume" loss channel, *J. Geophys. Res. Space Physics*, *119*, 9702–9713, doi:10.1002/2014JA019994.

Received 17 MAR 2014
Accepted 27 OCT 2014
Accepted article online 29 OCT 2014
Published online 9 DEC 2014

Mars Express observations of high altitude planetary ion beams and their relation to the "energetic plume" loss channel

Michael W. Liemohn[1], Blake C. Johnson[1], Markus Fränz[2], and Stas Barabash[3]

[1]Department of Atmospheric, Oceanic, and Space Sciences, University of Michigan, Ann Arbor, Michigan, United States, [2]Max-Planck Institute for Solar System Research, Katlenberg-Lindau, Germany, [3]Swedish Institute for Space Physics, Kiruna, Sweden

Abstract This study presents observational evidence of high-energy (ions >2 keV) beams of planetary ions above Mars' induced magnetospheric boundary (IMB) and relates them with the energetic plume loss channel calculated from numerical models. A systematic search of the Mars Express (MEX) ion data using an orbit filtering criteria is described, using magnetometer data from Mars Global Surveyor (MGS) to determine the solar wind motional electric field (Esw) direction. Two levels of statistical survey are presented, one focused on times when the MEX orbit was directly in line with the Esw and another for all angles between the MEX location and the Esw. For the first study, within the 3 year overlap of MGS and MEX, nine brief intervals were found with clear and unambiguous high-energy O^+ observations consistent with the energetic plume loss channel. The second survey used a point-by-point determination of MEX relative to the E-field and contained many thousands of 192 s measurements. This study yielded only a weak indication for an Esw-aligned plume. Furthermore, the y-z components of the weighted average velocities in the bins of this y-z spatial domain survey do not systematically point in the Esw direction. The first survey implies the existence of this plume and shows that its characteristics are seemingly consistent with the expected energy and flight direction from numerical studies; the second study softens the finding and demonstrates that there are many planetary ions beyond the IMB moving in unexpected directions. Several possible explanations for this discrepancy are discussed.

1. Introduction

Numerical models of the Mars space environment [e.g., *Luhmann and Schwingenschuh*, 1990; *Kallio and Koskinen*, 1999; *Boesswetter et al.*, 2004; *Modolo et al.*, 2005; *Harnett and Winglee*, 2006; *Brecht and Ledvina*, 2006; *Kallio et al.*, 2006b; *Fang et al.*, 2008; *Li and Zhang*, 2009; *Najib et al.*, 2011] predict two primary channels for the escape of planetary ions to deep space: a relatively low-energy population (near or below 1 keV) leaving via the central tail region, directly behind the planet, and an accelerated (well above 1 keV) loss in the direction of the solar wind motional electric field ($\mathbf{E}_{SW} = -\mathbf{U}_{SW}x\mathbf{B}_{IMF}$, where $\mathbf{B}_{IMF}$ is the interplanetary magnetic field). Observations of planetary ion loss at Mars, however, are dominantly focused on the former [e.g., *Lundin et al.*, 1989, 2004; *Barabash et al.*, 1991, 2007; *Dubinin et al.*, 1996, 2006; *Fedorov et al.*, 2006; *Nilsson et al.*, 2011, 2012]. Most of these measurements yield total escape rates similar to the central tail loss rates from the numerical models, within a rather large margin of uncertainty of up to factor of five [see, e.g., *Brain et al.*, 2010]. Note that novel combinations of plasma observations, such as the *Fränz et al.* [2010] usage of radio sounding densities and ion spectrometer velocities, yield a much larger loss rate of very low-energy ions down the central tail region.

Kallio et al. [1995] showed a few examples of Phobos-2 measurements of O^+ ions at energies >5 keV escaping from Mars, concluding that these are accelerated pick-up ions from the dayside magnetosheath region. *Kallio and Koskinen* [1999] compared one of these cases to test particle results, demonstrating the connection of the energetic plume to a dayside magnetosheath source. More recently, *Kallio et al.* [2006a, 2008] and *Boesswetter et al.* [2007] compared Mars Express (MEX) ion data with hybrid modeling results, with the model results clearly showing an energetic plume of planetary ions in the $+\mathbf{E}_{SW}$ direction while the data had, at most, hints of this population but were not fully conclusive.

Numerical models show that the energized planetary ion escape loss channel is created by the strong electric fields in the Mars magnetosheath, rapidly accelerating any heavy ions in this region. The gyroradius of a 1 keV

O^+ ion in a 3 nT magnetic field is 1.8 R_M (with a gyroperiod of 6 min); planetary ions within the + $\mathbf{E}_{SW}$ half of the magnetosheath stay in the solar wind-dominated region of near-Mars space, above the induced magnetosphere boundary (IMB). Because of Mars' small gravity and extended exosphere, ionization of the neutrals within the sheath is significant [cf., *Kallio and Koskinen*, 1999; *Fang et al.*, 2010b; *Curry et al.,* 2013a, 2013b]. Some models predict that this high-altitude source (as opposed to ionospheric outflow) dominates the loss of O^+ from Mars, through both escape channels [e.g., *Liemohn et al.*, 2013]. For half the magnetosheath (the side opposite the direction of + $\mathbf{E}_{SW}$), these particles either escape through the central tail or bombard the upper atmosphere of Mars [e.g., *Luhmann and Kozyra*, 1991; *Kallio et al.*, 2006b; *Fang et al.*, 2013]. On the other side of the magnetosheath, in the direction of + $\mathbf{E}_{SW}$, planetary ions will quickly leave near-Mars space. Pick-up ions are accelerated transversely to the solar wind flow, and the resulting cycloid motion moves them beyond the bow shock at or near the terminator [e.g., *Luhmann and Schwingenschuh*, 1990; *Kallio and Koskinen*, 1999; *Fang et al.*, 2008]. The sheath electric fields focus the heavy ions into a spatially confined plume within a few degrees of the $\mathbf{E}_{SW}$ clock angle, θ_E (the angle within the dawn-dusk, or terminator, plane, is important because $\mathbf{U}_{SW}$ is predominantly in the -x Mars Solar Orbital, or MSO, direction). The resulting narrow band of energetic ions has a front edge of highest-energy particles (well above a keV) near the terminator and an extended fan of gradually decreasing-in-energy particles extending back into the central tail loss channel [e.g., Figures 4 and 5 of *Fang et al.*, 2010a]. Where this energetic plume crosses the terminator, the energy and flight direction of the escaping O^+ are a focused, nongyrotropic beam in velocity space that changes with altitude. According to *Curry et al.* [2013a], in the terminator plane in the direction of + $\mathbf{E}_{SW}$, at 1.5 R_M altitude the beam is below 1 keV and traveling at an angle of $>$45° tailward from vertical, while at 2.3 R_M altitude the beam peak is above 5 keV and flowing nearly vertical with just a slightly tailward tilt.

Several studies with the MEX ion data set have focused on energetic beams of planetary ions escaping from Mars. *Dubinin et al.* [2006] analyzed nine MEX orbit segments with ascending or descending energies of planetary ions within the Mars magnetosphere. Only one of the events was beyond the IMB; not surprisingly, this was the one extending to the highest energies (up to 7 keV), appearing as an anomalous interval among the selected events (all of the other beams had a maximum energy below 2.5 keV). *Carlsson et al.* [2006, 2008] analyzed 150 ion beam observations, finding that their location with respect to Mars was organized by IMF, just as the modeled energetic plume should be. However, all of these beams were within the IMB and below 1 keV in energy.

Edberg et al. [2009] used Rosetta observations to provide the solar wind conditions in the vicinity of Mars to conclusively show that energetic (100 eV–10 keV) planetary ions were escaping in the + $\mathbf{E}_{SW}$ direction. The study showed two MEX orbits with energetic planetary ions beyond the IMB, flowing away from Mars in the + $\mathbf{E}_{SW}$ direction. The energy of the particles increased with distance from the planet and also increased on the second orbit when the solar wind dynamic pressure was higher. While not a systematic survey, the study conclusively demonstrated the existence of this energetic plume loss channel in the MEX data set.

Another set of studies that hint at the energetic plume loss channel of planetary ions are the $>$50 keV measurements from Phobos 2 [e.g., *Afonin et al.*, 1989; *Verigin et al.*, 1991; *McKenna-Lawlor et al.*, 1993]. These observations were not mass resolved, though, and could not conclusively state that the particles being detected were escaping planetary ions.

The only statistical survey study, thus far, that has presented clear observations of planetary ion beams consistent with the energetic plume from the MEX data is *Dubinin et al.* [2011]. This review of charged particle energization and escape around Mars and Venus contains a section on "ion pick-up" that includes an examination of observations in the magnetosheath (that is, between the IMB and the bow shock). They show that there are significant deviations between the planetary ion flow directions and that of the protons, traveling more radially away from Mars than the reaccelerating solar wind.

In the context of the numerical modeling results, the *Dubinin et al.* [2006] and *Carlsson et al.* [2006, 2008] analysis of ion beams in the tail region behind Mars is related to the magnetosheath source population and the energetic plume of escaping planetary ions, but those studies only considered the very lowest-energy and most tailward part of the loss channel fan. The *Dubinin et al.* [2011] section on pick-up ions presents measurements of beams within the energetic plume, but that study only gave an initial survey of possible observations. This study presents the results of a systematic examination for ion beams consistent with the front edge of this plume within the ion data set from MEX.

2. Data Sets

The primary data set for this study is that from the ion mass analyzer (IMA), part of the Analyzer of Space Plasma and Energetic Atoms (ASPERA-3) instrument suite onboard MEX [*Barabash et al.*, 2004, 2006]. The IMA instrument measures ions of 1–80 amu/charge in the energy range 10 eV to 32 keV/charge with an energy resolution of 8%. IMA has a field of view (FOV) that extends 360° in azimuth and 90° in polar angle, ±45° from the instrument detector plane, divided into 16 sectors in each angular direction. To provide adequate counting statistics in each energy and angle bin, IMA takes 192 s to conduct a full sweep through energy and polar angle. For this analysis, a robust calibration filter is applied that cleans the heavy ion mass channels of any contamination from stray H^+ counts by truncating the counts in certain channels to the average of the two neighboring channel count values. However, this procedure could also remove real O^+ counts. Therefore, the values below should be considered minimum count rates.

MEX is in a high-inclination orbit that annually precesses around the planet but with periapsis remaining relatively close to the equator. At high altitude, the region of interest for this study, MEX is oriented for optimal telemetry, leaving the IMA detector plane close to parallel with the ecliptic plane [*Barabash et al.*, 2006].

MEX did not carry a magnetometer, and while a method has been developed to determine the IMF clock angle, θ_{IMF}, from IMA-measured ion cycloid motion upstream of the bow shock [*Yamauchi et al.*, 2007], observations of upstream protons are rarely available due to the duty cycle and usual operational mode of the instrument. Therefore, for this study, θ_{IMF} values are taken from Mars Global Surveyor (MGS) magnetometer data [*Acuña et al.*, 1992]. MGS spent most of its mission lifetime in a 400 km altitude circular sun-synchronous orbit, and *Brain et al.* [2006] developed a method for estimating θ_{IMF} from the dayside northern hemisphere measurements in the magnetic pileup region. They produced a 2 h cadence data set (once every MGS orbit) of θ_{IMF} values from 1999 to the end of the MGS mission in November 2006. MEX reached Mars in late 2003 and IMA began returning scientific data in January 2004. Therefore, a 2 year, 10 month overlap exists between the MEX-IMA and MGS-derived θ_{IMF} data sets. This data set of IMF draping angles has been used extensively with MEX ion and electron observations [e.g., *Carlsson et al.*, 2008; *Dubinin et al.*, 2008; *Nilsson et al.*, 2011; *Wang et al.*, 2013; *Dieval et al.*, 2014].

3. Analysis

Two statistical surveys are presented below. The first focuses on times when the MEX orbit was aligned within a narrow spatial window of the + $\mathbf{E}_{SW}$ direction and beyond the IMB. Two-hour intervals of the MEX orbit are then examined for high counts of energetic planetary ions. The second survey considers the instantaneous location of MEX and calculates its position in Mars-Solar-Electric (MSE) coordinates, i.e., relative to the + $\mathbf{E}_{SW}$ direction. Each 192 second IMA measurement above the IMB is classified separately, resulting in a much bigger database of observations.

3.1. Spatially Confined Survey

A search was conducted for all intervals when θ_E, which is 90° counterclockwise (as viewed from the Sun) from θ_{IMF}, was within 5° of the MEX orbit plane. Orbital normal vectors, $\mathbf{o_n}$, were computed for each 2 h orbit segment and then compared against the corresponding θ_{IMF} value. If the angle of $\mathbf{o_n}$ in the y-z plane is within 5° of an MGS θ_{IMF} value then that 2 h interval of MEX orbit was flagged for additional examination. The alignment could be parallel or antiparallel vectors, as either one might result in an energetic plume observation. This search found 512 intervals of potential observation of the energetic plume. IMA has a restricted operational mode, however, and only 214 of these 2 h intervals have usable heavy ion data. Furthermore, MEX must be in the proper portion of the orbit, namely on the + $\mathbf{E}_{SW}$ side near the terminator above the IMB. This position filter left only 57 possible 2 h intervals of observations. Among these, nine intervals contain a definitive measurement of the energetic plume with strong heavy ion fluxes above 2 keV.

Figure 1 highlights one of the seven energetic plume intervals, showing three projections of the MEX orbit from 9 October 2005 for the 2 h interval from 16:30 to 18:30 UT. The MGS-derived θ_E estimate of 70° was made in the middle of this interval. The circle in each plot represents Mars, and the red and green curves show an empirical estimation of the IMB and the bow shock, respectively, from *Trotignon et al.* [1996]. Overplotted along the orbit trajectory is the number of IMA counts attributed to 2–10 keV O^+ detection.

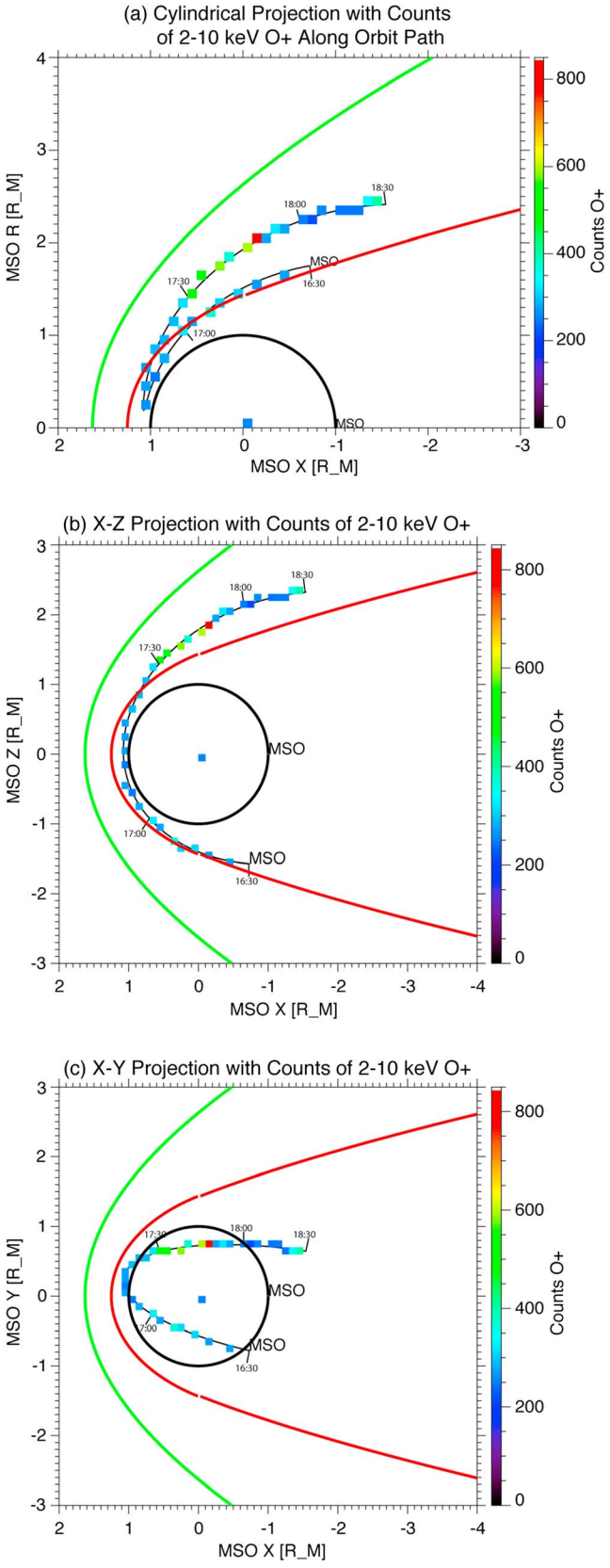

MEX is located above the north polar region and slightly duskward, with a strong burst of energetic O^+ counts as MEX crossed the terminator. The total count rate peaks in the ~800 range, indicating that the statistics for these observations are robust. For this location, test particle results predict that the energetic plume should be between 3 and 8 keV and flowing mostly northward with a slight duskward component and tailward tilt of 40–60° with a directional flux peaking in the range of ~10^6 ions $cm^{-2}\,s^{-1}\,sr^{-1}$ for nominal solar wind conditions [cf. Figure 3 of *Kallio et al.*, 2008, and Figures 7 and 8 of *Curry et al.*, 2013a].

Figure 1 includes empirically derived locations of the IMB and bow shock, but the IMB can vary dramatically, especially away from the subsolar region (i.e., near the terminator) [e.g., *Vignes et al.*, 2000]. Fortunately, MEX data can be used to determine if the spacecraft is beyond the IMB for the particular interval of energetic O^+ observation. Figure 2 shows energy-time spectrograms for the 16:30 to 18:30 UT interval on 9 October 2005 for electrons, protons, and oxygen ions. During periapsis, MEX was on the dayside and passed below the IMB. The transitions out of and back in to the magnetosheath are clearly seen in the electron and proton spectrograms, with the outbound crossing occurring at 17:20 UT. The satellite therefore is definitely in the magnetosheath at the time of the energetic O^+ measurements from 17:30 to 17:50 UT. A comparison of Figures 2b and 2c also shows that the high fluxes in the O^+ spectrogram do

Figure 1. Mars Express (MEX) orbit during an interval of interest on 9 October 2005, projected into the Mars Solar Orbital (MSO) x-R_{yz}, x-z, and x-y coordinate planes, where R_{yz} is the cylindrical distance from the x axis. The green and red curves show empirical locations of the bow shock and induced magnetospheric boundary (IMB), respectively. The colored dots along the orbit indicate the total >2 keV O^+ counts during each ion mass analyzer (IMA) velocity space sweep. Distances are given in Mars radii, and UT tickmarks are shown every 30 min along the orbit path.

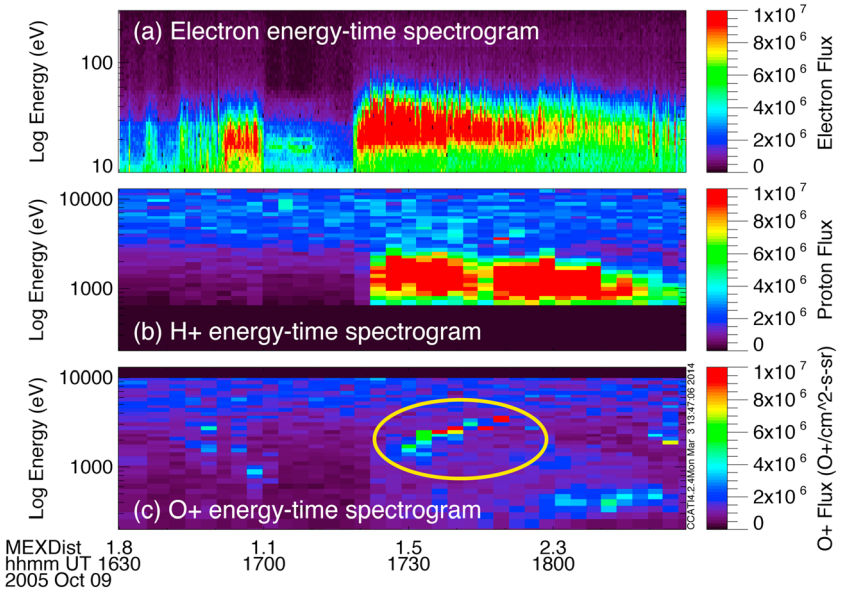

Figure 2. Energy versus time spectrograms of MEX observations during the 2 hour interval on 9 October 2005, integrated over the angular field of view (FOV), for (a) electrons, (b) protons, and (c) oxygen ions. The yellow oval in the O^+ spectrogram highlights the observation of interest.

not correspond to any similar feature in the H^+ spectrogram, implying that the oxygen ion measurements are, in fact, O^+ and not a spurious signal from the coincident high flux of H^+. Finally, Figure 2 is shown in units of directional number flux, with all three plots on the same linear scale. It is seen that the O^+ values are in the range of several times 10^6 ions $cm^{-2}\,s^{-1}\,sr^{-1}$, approaching 10^7 at the peak times.

Figure 3 presents a velocity-space analysis of this event. Figure 3a, which shows the energy-time spectrogram for this interval, reveals a strong count rate of 3–4 keV O^+ from 17:33 to 17:50 UT, with the highest rates seen near the end (before the O^+ signal disappears). This plot shows that the counts within each energy bin (although summed over flight direction) are over 100 in the high flux region of interest. Figure 2b shows $>$2 keV ion counts as a function of time and mass channel in the instrument. Oxygen ions at these energies should be centered in mass channel 5. However, mass channels 1 and 5 are highly susceptible to ghost counts of energetic H^+, which should be centered at channel 25. For an unambiguous determination of O^+, the counts should not be isolated to only channel 5, but rather should show a spread across several adjacent mass channels. Examination of Figure 3b between 17:30 and 17:50 reveals that the high-energy counts are indeed O^+. Figure 3c displays the $>$2 keV O^+ count rate versus FOV angles at 17:50 UT, showing that the highest flux enters at the smallest polar angle and a slightly positive azimuthal angle. Because a polar angle of 90° is in the ecliptic plane, these particles are traveling mostly upward (northward) and a bit tailward and duskward. Note that the count rates in this particular section of the flight direction grid range from 20 to 120, again indicating that the statistics are sufficient to confidently identify this observation as a real measurement of an energetic O^+ beam within the magnetosheath.

To further illustrate and investigate this, Figure 4 shows the influence on the results of the chosen calibration method within the IMA data-processing software. The left column shows O^+ energy versus time spectrograms while the right column contains mass channel versus time spectrograms summed over the 2–10 keV energy range. The top row used the "standard" calibration setting while the lower panel has the extra-clean calibration setting that aggressively removes H^+ spurious counts. Note that the color scales are linear and slightly different between the two columns. Comparing Figures 4a and 4b shows that the supposedly O^+ fluxes in the 7–10 keV range are removed with the enhanced calibration technique, but the fluxes of interest within the 3–4 keV range are only slightly altered. A comparison of the mass-time spectrograms in Figures 4c and 4d shows that the bright streak of counts in mass channel 5 (and others) is removed, leaving the high flux values in the O^+ mass channel range in the 17:30–17:50 UT time interval.

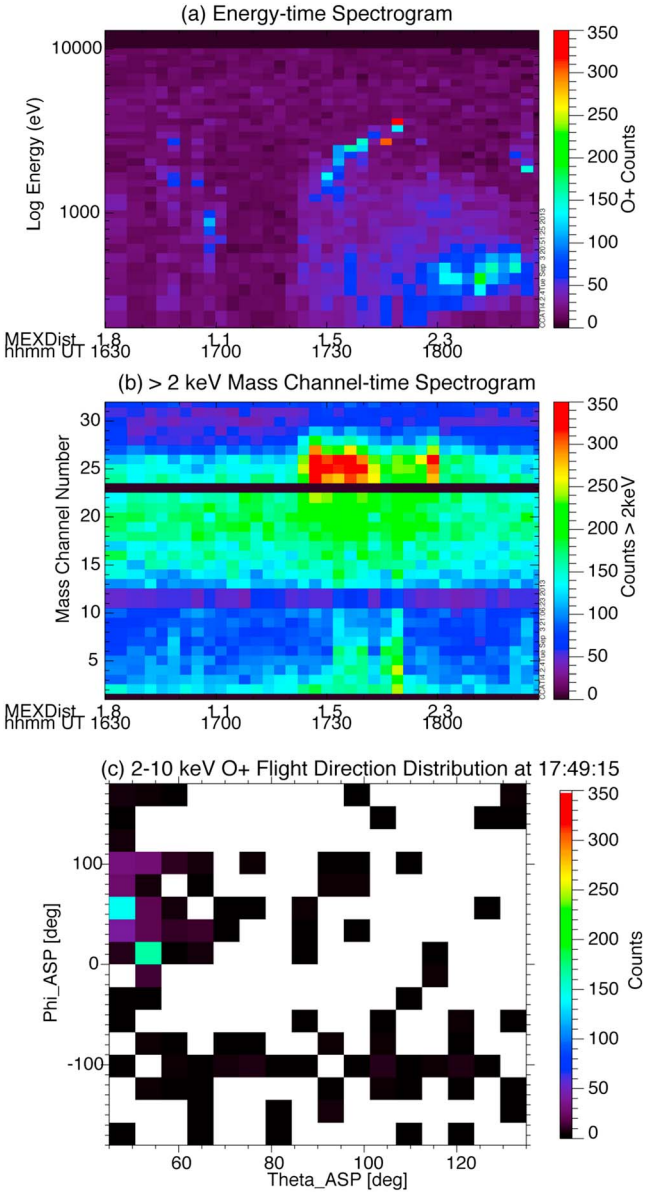

Figure 3. (a) Energy versus time spectrogram of IMA O^+ data during the 2 hour interval on 9 October 2005, integrated over the angular FOV. (b) Mass channel versus time spectrogram during the interval for particles above 2 keV in energy. (c) IMA azimuth versus polar angle counts of O^+ during one IMA sweep interval (at 17:50 UT), integrated over 2–10 keV.

Table 1 inventories the intervals of energetic plume observation. Listed are the start and end times (to the nearest 10 min), the time of the closest MGS value for the IMF clock angle, MEX's Mars-centric distance and its distance to an empirical IMB location, the observed energies of the flux peak, and θ_E for this interval, measured relative to the $+y_{MSO}$ direction going counterclockwise as viewed from the Sun, as well the preceding and following θ_E values. The correlations of start and end values of energy versus MSO and IMB distance are weak (0.19 and 0.43, respectively), and only the latter is statistically significant.

Supplemental figures are provided for all nine of these events, showing the orbit configuration with energetic O^+ counts along the satellite track, energy-time spectrograms (including electron and proton spectrograms to confirm MEX was in the sheath, the mass channel versus time plots revealing the high count rates in the O^+ channels, and figures with and without the application of the extra-clean calibration technique to demonstrate the removal of proton contamination. In these supplemental figures, it is seen that all nine include strong count levels of O^+ above 2 keV in energy. Many of these observations are made at or near the edge of the polar angle extent of the IMA instrument. In addition, seven of the nine observations are clearly above the IMB and within the magnetosheath, as evidenced by the coexistence of solar wind electrons and protons at the times of the energetic oxygen ion observations. The other two might be above the IMB, but the electron and proton data make this conclusion ambiguous.

3.2. Survey of All Relative Angles

The first survey presented above only considered a rather limited spatial domain when MEX was beyond the IMB and within a very narrow angular extent relative to the $+\mathbf{E}_{SW}$ direction. Extended (2 h long) intervals of the MEX orbit were examined for evidence of planetary ions resembling the energetic plume loss channel. This is not the only methodology for assessing the existence of the energetic plume in the IMA data set, however. Another technique was also used, and the results of this second survey are presented below.

For this analysis, instead of calculating the relative angle of the MEX orbital plane with $\mathbf{E}_{SW}$, the location of MEX during each individual IMA measurement beyond the *Trotignon et al.* [1996] empirical IMB was categorized relative to the electric field. This greatly increased the number of measurements in the assessment because all orbital planes are included and not just those closely aligned with $\mathbf{E}_{SW}$. To organize the ion fluxes relative to $\mathbf{E}_{SW}$,

Table 1. Intervals of Energetic O^+ Plume Observation When the Mars Express (MEX) Orbit Plane Was Aligned With 5° of the Mars Global Surveyor (MGS)-Derived E_{SW} Clock Angle (Measured Counterclockwise From Dusk)

Date	Start UT	End UT	UT of θ_E	Mars Solar Orbital (MSO) Dist. in R_M	Dist. to Induced Magnetospheric Boundary (IMB) in R_M	E Range in keV	θ_E	Prior θ_E	Next θ_E	In Sheath?
01 Aug 2004	04:40	04:50	04:49	1.7–1.9	0.4–0.6	2–3	197°	124°	71°	Yes
12 Dec 2004	11:00	11:50	11:46	1.5–2.8	0.2–0.3	4–7	301	214	314	Yes
15 Apr 2005	04:20	04:30	05:03	2.2–2.7	0.2–0.5	2–3	306	10	332	Maybe
03 Jun 2005	05:30	06:00	06:32	1.5–2.1	0.1–0.8	4–9	152	242	333	Yes
10 Jun 2005	05:50	06:00	05:21	2.1–2.4	0.6–0.9	2–5	351	4	151	Yes
09 Oct 2005	17:30	17:50	17:30	1.5–2.0	0.3–0.5	3–4	70	135	28	Yes
02 Apr 2006	22:30	22:50	22:43	1.3–1.5	0.0–0.2	2–4	347	26	0	Yes
10 Jul 2006	19:50	20:00	19:07	2.5–2.6	0.2–0.2	2–3	288	154	304	Maybe
23 Jul 2006	01:30	01:40	01:28	2.1–2.6	0.3–0.3	2–3	103	72	109	Yes

the same 2004–2006 interval was used for this part of the analysis as was done above. Furthermore, only measurements taken within ±30 min of the MGS draping angle proxy are considered for this assessment. MEX orbit times with no IMA were not counted, nor were IMA data for which the calculated velocity moment was either exactly zero or larger than the speed of light (indicating spurious data values). This survey yielded ~28,000 measurements (each 192 s long) of good IMA ion observations with both H^+ and O^+ fluxes.

Figure 5 presents an overview of this measurement collection. The coordinate system in the panels is the MSE y-z plane, with values integrated or averaged over the x dimension. The view is from the Sun, and the size of Mars is shown as a black circle in the middle of each panel. The grid resolution was set to 0.4 R_M; this is a

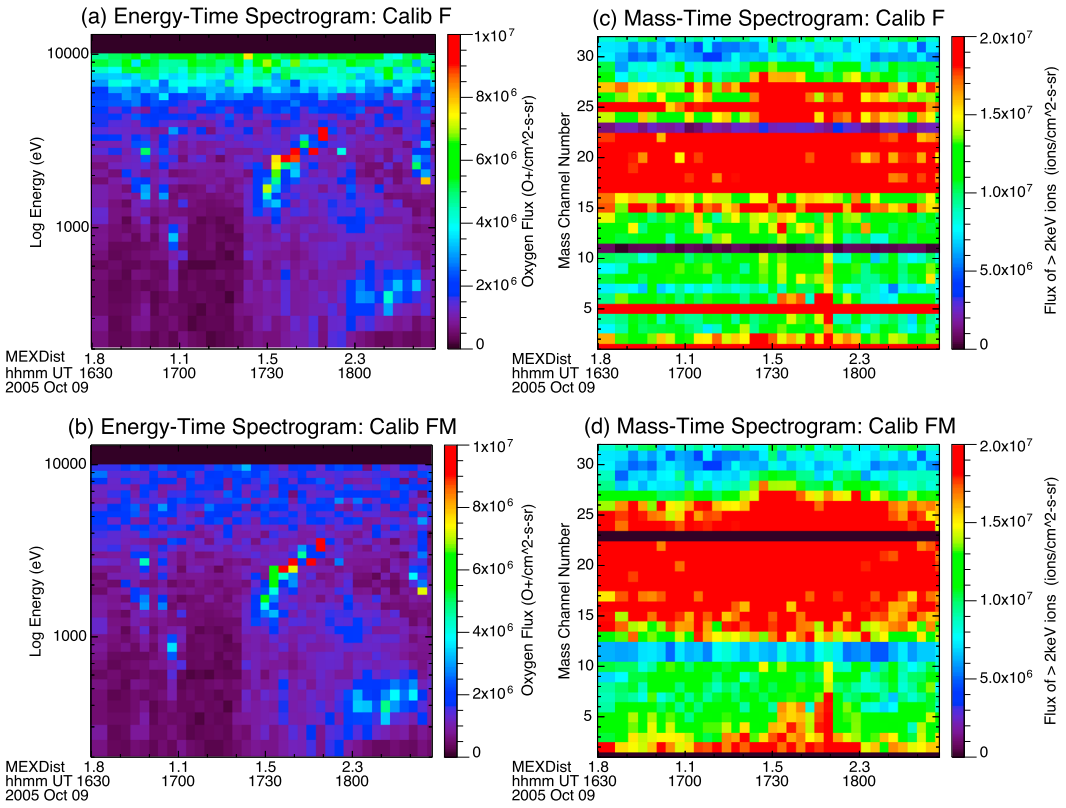

Figure 4. Planetary O^+ data for 9 October 2005, like Figure 3 except in units of directional number flux instead of counts and showing the difference between instrument calibration methods. Shown are the following: (a) energy-time spectrogram of IMA O^+ with the "standard" calibration; (b) energy-time spectrogram with the enhanced calibration to remove spurious H^+ counts in the O^+ mass channels; (c) mass channel versus time spectrogram for particle energies above 2 keV with the standard calibration; and (d) mass channel versus time with the enhanced calibration.

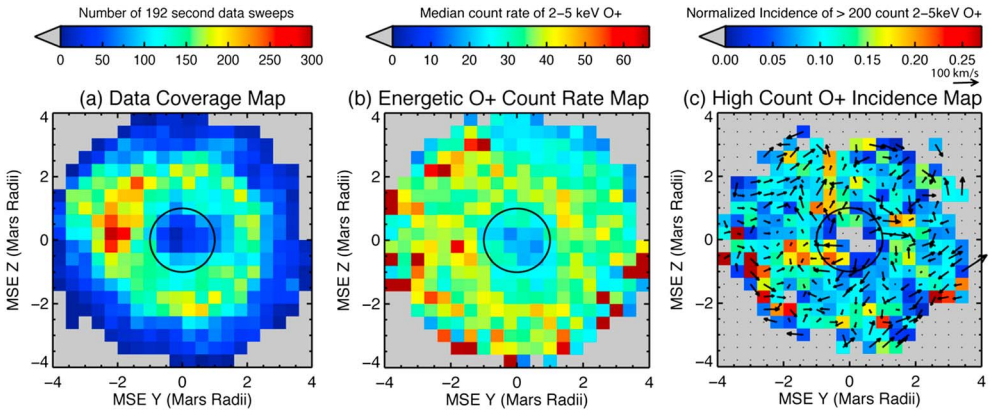

Figure 5. Survey results of all IMA data beyond the IMB. Each panel shows values in the MSE y-z plane, with the view from the Sun towards Mars and the planetary outline shown as a black circle. Shown are the following: (a) the total count of unique IMA measurements in the selected spatial domain (i.e., beyond the IMB); (b) the median count rate of 2–5 keV O^+; and (c) the occurrence rate of 2–5 keV O^+ with counts higher than 200. In Figure 5c, weighted average velocity vectors are shown for each bin. The grid resolution used for this survey is 0.4 R_M, summing or averaging over the x position values.

somewhat arbitrary value chosen to provide statistical significance yet still offer spatial resolution. Note that each plot contains different values and therefore has its own colorscale.

Figure 5a shows the data coverage map. This is the count of all IMA measurements beyond the IMB in that y-z grid cell. This plot reflects the characteristics of the MEX orbit, with apoapsis usually near the equatorial plane, and the duty cycle of IMA, which is often turned off at high altitudes. There is a clear gap in coverage near the center of the plot; this location is upstream of the Mars subsolar region, when MEX is near apoapsis and IMA is rarely operating. The coverage is fairly good, though, in an annulus from 1 to 3 R_M cylindrical distance from the x axis. These measurements are mostly in the magnetosheath region within ±1 R_M of x = 0, but they also contain observations beyond the bow shock. The grid resolution was chosen to yield total measurement values over 100 in this region to provide adequate counting statistics and reasonable error values to the results.

Figure 5b gives the median count value of O^+ in the 2–5 keV energy range. Interestingly, the higher values occur at the larger cylindrical distances, while the region of interest closer to Mars (the high data coverage annulus seen in Figure 5a) has a fairly uniform median count rate of roughly 40. This is because no filtering was conducted to remove times with only noise in the energetic O^+ velocity distribution. Because each O^+ count rate measurement is actually a summation over a few energy channels and all flight direction bins, a count rate of 40 very well could be down in the noise. That is, in examining Figure 3c, each black square in this flight direction plot indicates that there is at least one and perhaps several counts in that bin.

To isolate the measurements with a physically meaningful count rate of energetic O^+, a filter was applied to only consider those observations with more than 200 O^+ counts in the 2–5 keV energy range. This value was chosen somewhat arbitrarily, but Figures 1 through 4 (and the supplemental figures) suggest that this is a good threshold to remove the noise-only measurements from the data set. Figure 5c presents values for the occurrence rate of these high-count-rate measurements (a simple ratio against the data coverage value in Figure 5a). Gray regions indicate no measurement intervals of high-count energetic O^+. The total number of measurements with high-count energetic O^+ is just under 2800, about 10% of the total measurement number in the selected data set. Overplotted on the colored bins are y-z component vectors of the weighted-average velocity from these high-count O^+ observations. Specifically, the velocity value for a particular measurement was multiplied by the corresponding count rate, these values were then summed for all data in the grid cell, and this value was divided by the sum of the count rates in that cell.

The incidence rate map in Figure 5c reveals that the measurements of high-count O^+ are not restricted to the + $\mathbf{E}_{SW}$ direction. While there is a column of relatively higher incidence rates of ~0.2 along the + z axis, there are also many grid cells of similarly high occurrence rate elsewhere in the map. Most of the values in the annulus of high data coverage are between 0.1 and 0.2, and no strong preference is seen relative to $\mathbf{E}_{SW}$.

A second feature of Figure 5c is that the y-z component velocity vectors of high-count energetic O^+ are not systematically aligned in the $+\mathbf{E}_{SW}$ direction. In the column of higher incidence rates along the +z axis, the vectors tend to point in the +z direction, indicating a preference for outward flow. However, many other vectors in high occurrence rate grid cells are not aligned with $+\mathbf{E}_{SW}$. Around the annulus of high data coverage, the vectors show no preferred direction and, on average, are pointed randomly.

It should be noted that a 2 keV O^+ ion has a total velocity of ~150 km/s. The fact that all of the vectors in Figure 5c are smaller than this value is reasonable, however. First, the x component of the velocity is not included in this vector, and therefore any tailward motion of the ions is not shown in this plot. Second, the observed flight directions include ions traveling in both the positive and negative y and z directions, and these weighted averaged velocities take into account the sign of the components in the summation.

4. Discussion

From the first survey of the MEX ion data, several cases were found of energetic (E >2 keV) planetary O^+ flowing outward from the dayside region in the direction of $+\mathbf{E}_{SW}$. From the second survey, the median and weighted average results do not show a particular preference for an energetic plume in the direction of $+\mathbf{E}_{SW}$. Several implications and caveats about these findings need to be addressed.

The main inference to make from the first survey is that the models, to some degree, were correct in their predictions of this energetic plume. That is, the plume exists in near-Mars space, and its characteristics roughly correspond to what the models yield for this population of escaping ions. However, the plume is not present all of the time in the MEX ion data set when MEX is in the proper location to observe it.

The main finding to draw from the second survey is that the high-altitude energetic O^+ ions are not clearly and systematically flowing away from Mars in the direction of $+\mathbf{E}_{SW}$. While there is an evidence for a higher occurrence rate of generally outward flowing energetic O^+ ions in a narrow column close to the $+z_{MSE}$ axis, this is not the only place for high occurrence rates, and the overall pattern of the velocities is not organized by the electric field.

Detection of O^+ beams consistent with the energetic plume of planetary ion loss from Mars has been problematic for several reasons. The first is the time variation of the IMF, which regularly changes direction and is very rarely stable for an entire 2 h interval. The transit time for the solar wind and IMF to sweep past Mars is on the order of a minute or two, and so the magnetic environment around Mars reconfigures very quickly with the passage of a new θ_{IMF}. IMF variability could explain why only a small fraction of the possible observation intervals contained a clear signal of high-altitude energetic O^+.

A second obstacle to observation is the MEX orbit, which has characteristics that systematically impede observation of this population. The typical orientation of the IMF is in a Parker spiral configuration, with the IMF confined near the equatorial plane. This means that the typical $\mathbf{E}_{SW}$ vector points either northward or southward, and the optimal location to view energetic plume beams is high above the Mars polar regions. The MEX orbit, with apoapsis near the equatorial plane, means that the spacecraft is often not at a high altitude when crossing the terminator plane.

A third impediment is the IMA duty cycle, with the instrument often inactive during the orbit segments most likely to contain this population. This lowers the total number of possible measurements at high altitudes therefore the number of possible energetic plume observations in the MEX data set.

Fourth, the IMA FOV orientation relative to Mars is such that the plume is often in the "FOV hole" when MEX is within the expected plume region. Only when the energetic plume beam is less vertical and tilted towards the tailward direction is observation possible. For example, in the case highlighted in the first survey, the detection was made at the edge of the polar angle extent of IMA's FOV, indicating that there could have been additional planetary ions with more vertical flight directions that were not observed by the instrument. This could also explain why only a small fraction of the possible observation intervals contained outflowing energetic O^+ signals.

A fifth issue is that some the IMA mass channels that are supposed to detect high-energy O^+ are sometimes contaminated by ghost signals from H^+. This means that the planetary ion flux needs to be quite strong in order for the counts from IMA to be clearly identified as O^+. Furthermore, the calibration method possibly

removes O^+ counts when MEX is at high altitudes in the sheath and solar wind, as described in section 2 above, leaving an underestimation for this population.

Finally, an issue of this particular analysis is the uncertainty in θ_{IMF} from MGS. The median change in θ_{IMF} from this data set is 44°. Even if the IMF is steady, variations within the ionosphere could create additional draping of the magnetic field at MGS altitudes and change the θ_{IMF} estimate. This is another reason for the low observation rate in the candidate intervals of the first survey and the inconclusive statistics of the second survey.

A counterhypothesis that should be mentioned is that numerical models predicting this energetic plume of escaping planetary ions could be incorrect. While it is seen in multi-fluid MHD models [e.g., *Najib et al.*, 2011], hybrid models [e.g., *Boesswetter et al.*, 2004; *Brecht and Ledvina*, 2006], and test particle models [e.g., *Luhmann and Schwingenschuh*, 1990; *Liemohn et al.*, 2013], each of these simulation configurations has their limitations [cf. review by *Ledvina et al.*, 2008 and model comparison by *Brain et al.*, 2010]. For instance, MHD modeling assumes that the particles maintain a drifting Maxwellian velocity space distribution function, and this assumption breaks down in the non-gyrotropic flows present in the energetic plume. Furthermore, MHD models do not include the microphysical scattering processes, such as wave excitation and wave-particle interactions, which could alter the velocity space distribution and therefore change the trajectory of the planetary ions. Turbulent fluctuations of the magnetic field and bulk flow velocity in the sheath region are probably not fully captured in large-scale modeling simulations, and the presence of such small-scale or sub-grid variations would introduce a level of randomization in the pick-up ion velocity. Hybrid models include non-gyrotropic ion motion, but they rely on the summation of macroparticle weightings to reconstruct the velocity space distribution and counting statistics are usually poor for planetary ions at high altitudes. While the self-consistent electrodynamic calculation within hybrid models is capable of representing ion wave excitation and feedback, they usually have large grid cells that do not capture and reproduce these microphysical processes. Test particle models are capable of highly resolving velocity space, but they lack self-consistency in the electric and magnetic fields through which the particles are moving and therefore could be misrepresenting the true flow patterns. If the assumed E and B fields do not contain turbulent fluctuations in the sheath, then the calculated flow patterns could be, to some degree, unrealistic. Furthermore, they are often collisionless and therefore, like the other two modeling techniques, usually do not include the microphysical scattering processes. This is not to say that the modeling results are incorrect in predicting an energetic plume, it just means that the details of the plume in near-Mars space could be different from what is calculated from these simulation tools.

A result from the analysis in the first survey is that the energy of the escaping planetary ion beam was weakly correlated with the distance of the observation from the IMB. This correlation of energy with altitude was noted by *Dubinin et al.* [2011] and is predicted by the numerical models as the particles are accelerated as they move along $\mathbf{E}_{SW}$. The weakness of the correlation is expected given the uncertainty of the magnitudes of U_{SW} and B_{IMF} for each case. In addition, observations and modeling have shown a latitudinal dependence to the IMB [e.g., *Crider et al.*, 2002], including an influence of the crustal magnetic fields [e.g., *Ma et al.*, 2002; *Harnett and Winglee*, 2003; *Edberg et al.*, 2008].

While the two surveys presented above reach seemingly different conclusions about the existence of the energetic plume of escaping planetary ions, there are explanations that possibly resolve this apparent discrepancy. First, the two studies used different measurement selection criteria: one considered extended parts of orbits while the other classified each measurement as a separate contribution to the data set. Therefore, one survey is focused on finding intervals of beam outflow, while the other survey considered each unique measurement within such an interval as a different contribution to the statistics.

A second difference between the surveys in the orbit selection criteria: one considered only those orbits aligned with $\mathbf{E}_{SW}$, while the other allows all orbit configurations. Therefore, orbits orthogonal to $\mathbf{E}_{SW}$ are included in the larger data set that were excluded in the first, more limited, survey.

Another possible source of the discrepancy is in the "event" selection criteria: the first survey made this assessment manually while the other considered a particular count rate threshold of 2–5 keV O^+. The first method is subjective but found several clear intervals of beam-like outflow flows of energetic O^+. The second method is more quantitative but the exact threshold level is a subjective choice, and noise-dominated measurements could be classified as high-count values and therefore negatively influence the statistics.

Finally, the two approaches apply different velocity space analyses: one examined the count rate in the flight direction grid and isolated the beam manually, while the other one conducted weighted averages of the average velocity from each measurement interval. The first is subjective in defining the beam within the flight-direction domain space, but allows for an examination and assessment of this beam relative to what is expected from numerical models. While the second method is more quantitative, noise-level counts are included in these averages that could be obscuring the flight direction of any beams in the data.

Therefore, the findings from the two surveys are not incompatible, but rather each needs to be considered within the specific limitations of that methodology.

5. Conclusion

Two systematic investigations of MEX ion data were conducted to identify observations consistent with the energetic plume of escaping planetary ions from Mars. The first investigation focused on times when the orbital plane of MEX was within 5° of the estimated IMF clock angle from MGS observations (determined once per MGS orbit) and also to when MEX was above the IMB. Of the 57 possible 2 h intervals for which MEX was in the correct place with available heavy ion data from IMA, nine cases of energetic ($E > 2$ keV) escaping planetary ions were found. The energy of the beam weakly correlates with distance from the IMB. One of these cases was presented in detail, revealing that the number flux, energy, and flight direction of the observed beam are consistent with the expectations from numerical models (as were the other cases).

The second survey separately classified each MEX ion measurement made beyond the IMB, calculating the instantaneous MEX position relative to $+\mathbf{E}_{SW}$ and applying specific thresholds for defining significant O^+ count rates. This study revealed a weak signature of an energetic plume in the direction of $+\mathbf{E}_{SW}$, but the results are not strongly conclusive and the findings are seemingly at odds with the first study. Several reasons were given above as to why the two surveys could yield disparate results.

In addition, numerous caveats were listed as to why the observations are so sparse within the MEX ion data set. Given the limiting conditions, only a few observations of front edge beams from the energetic plume were identified in the MEX IMA data. These intervals are not adequate to robustly quantify the magnitude of the total ion loss rate via the plume. The general conclusion of the two studies is that the energetic plume exists but it is not systematically and ubiquitously apparent in the high-altitude MEX data set.

Acknowledgments
The authors thank NASA and NSF for supporting this work, particularly under NASA grants NNX11AD80G, NNX13AG26G, and NNX14AH19G, and NSF grant AST-0908311. The data are available at the ASPERA-3 website at the Swedish Institute for Space Physics, http://aspera-3.irf.se/thedata, and have been processed and plotted using the CCATi software package written in IDL.

Larry Kepko thanks the reviewers for their assistance in evaluating the paper.

References

Acuña, M. H., et al. (1992), Mars Observer magnetic fields investigation, *J. Geophys. Res.*, *97*(E5), 7799–7814, doi:10.1029/92JE00344.
Afonin, V., et al. (1989), Energetic ions in the close environment of Mars and particle shadowing by the planet, *Nature*, *341*, 616–618, doi:10.1038/341616a0.
Barabash, S., E. Dubinin, N. Pisarenko, R. Lundin, and C. T. Russell (1991), Picked-up protons near Mars – PHOBOS observations, *Geophys. Res. Lett.*, *18*, 1805–1808, doi:10.1029/91GL02082.
Barabash, S., et al. (2004), The analyser of space plasmas and energetic atoms (ASPERA-3) for the European Mars Express mission, in *Mars Express: A European Mission to the Red Planet*, *ESA Publ. SP-1240*, edited by A. Wilson, pp. 121–139, Eur. Space Agency, ESTEC, Noordwijk, Netherlands.
Barabash, S., et al. (2006), The Analyzer of Space Plasmas and Energetic Atoms (ASPERA-3) for the Mars Express mission, *Space Sci. Rev.*, *126*, 113–164.
Barabash, S., A. Fedorov, R. Lundin, and J.-A. Sauvaud (2007), Martian Atmospheric Erosion Rates, *Science*, *315*, 501–503, doi:10.1126/science.1134358.
Boesswetter, A., T. Bagdonat, U. Motschmann, and K. Sauer (2004), Plasma boundaries at Mars: A 3-D simulation study, *Ann. Geophys.*, *22*, 4363–4379.
Boesswetter, A., et al. (2007), Comparison of plasma data from ASPERA- 3/Mars-Express with a 3-D hybrid simulation, *Ann. Geophys.*, *25*, 1851–1864.
Brain, D. A., D. L. Mitchell, and J. S. Halekas (2006), The magnetic field draping direction at Mars from April 1999 through August 2004, *Icarus*, *182*, 464–473, doi:10.1016/j.icarus.2005.09.023.
Brain, D., et al. (2010), First results from the SWIM Model Challenge, *Icarus*, *206*, 139, doi:10.1016/j.icarus.2009.06.030.
Brecht, S. H., and S. A. Ledvina (2006), The solar wind interaction with the Martian ionosphere/atmosphere, *Space Sci. Rev.*, *126*, 15–38, doi:10.1007/s11214-00609084-z.
Carlsson, E., et al. (2006), Mass composition of the escaping plasma at Mars, *Icarus*, *182*, 320–328.
Carlsson, E., D. Brain, J. Luhmann, S. Barabash, A. Grigoriev, H. Nilsson, and R. Lundin (2008), Influence of IMF draping direction and crustal magnetic field location on Martian ion beams, *Planet. Space Sci.*, *56*, 861–867, doi:10.1016/j.pss.2007.12.016.
Crider, D. H., et al. (2002), Observations of the latitude dependence of the location of the martian magnetic pileup boundary, *Geophys. Res. Lett.*, *29*(8), 1170, doi:10.1029/2001GL013860.
Curry, S. M., M. W. Liemohn, X. Fang, Y. Ma, A. F. Nagy, and J. Espley (2013a), The influence of production mechanisms on pickup ion loss at Mars, *J. Geophys. Res. Space Physics*, *118*, 554–569, doi:10.1029/2012JA017665.
Curry, S. M., M. W. Liemohn, X. Fang, D. Brain, and Y. Ma (2013b), Simulated kinetic effects of the corona and solar cycle on high altitude ion transport at Mars, *J. Geophys. Res. Atmos*, *118*, 3700–3711, doi:10.1002/jgra.50358.

Dieval, C., D. D. Morgan, F. Nemec, and D. A. Gurnett (2014), MARSIS observations of the Martian nightside ionosphere dependence on solar wind conditions, *J. Geophys. Res. Space Physics*, *119*, 2077–2093, doi:10.1002/2014JA019788.
Dubinin, E. M., K. Sauer, R. Lundin, K. Baumgärtel, and A. Bogdanov (1996), Structuring of the transition region (plasma mantle) of the Martian magnetosphere, *Geophys. Res. Lett.*, *23*, 785–788.
Dubinin, E., et al. (2006), Electric fields within the Martian magnetosphere and ion extraction: ASPERA-3 observations, *Icarus*, *182*, 337–342, doi:10.1016/j.icarus.2005.05.022.
Dubinin, E., M. Fränz, J. Woch, E. Roussos, S. Barabash, R. Lundin, J. D. Winningham, R. A. Frahm, and M. Acuña (2008), Plasma morphology at Mars: ASPERA-3 observations, *Space Sci. Rev.*, *126*, 209–238, doi:10.1007/s11214-006-9039-4.
Dubinin, E., M. Fraenz, A. Fedorov, R. Lundin, N. Edberg, F. Duru, and O. Vaisberg (2011), Ion energization and escape on Mars and Venus, *Space Sci. Rev.*, *162*, 173–211, doi:10.1007/s11214-011-9831-7.
Edberg, N. J. T., et al. (2009), Rosetta and Mars Express observations of the influence of high solar wind pressure on the Martian plasma environment, *Ann. Geophys.*, *27*, 4533–4545, doi:10.5194/angeo-27-4533-2009.
Edberg, N. J. T., M. Lester, S. W. H. Cowley, and A. I. Eriksson (2008), Statistical analysis of the location of the Martian magnetic pileup boundary and bow shock and the influence of crustal magnetic fields, *J. Geophys. Res.*, *113*, A08206, doi:10.1029/2008JA013096.
Fang, X., M. W. Liemohn, A. F. Nagy, Y. Ma, D. L. De Zeeuw, J. U. Kozyra, and T. Zurbuchen (2008), Pickup oxygen ion distribution around Mars, *J. Geophys. Res.*, *113*, A02210, doi:10.1029/2007JA012736.
Fang, X., M. W. Liemohn, A. F. Nagy, J. G. Luhmann, and Y. Ma (2010a), On the effect of the Martian crustal magnetic field on atmospheric erosion, *Icarus*, *206*, 130, doi:10.1016/j.icarus.2009.01.012.
Fang, X., M. W. Liemohn, A. F. Nagy, J. G. Luhmann, and Y. Ma (2010b), Escape probability of Martian atmospheric ions: Controlling effects of the electromagnetic fields, *J. Geophys. Res.*, *115*, A04308, doi:10.1029/2009JA14929.
Fang, X., S. W. Bougher, R. E. Johnson, J. G. Luhmann, Y. Ma, Y.-C. Wang, and M. W. Liemohn (2013), The importance of pickup oxygen ion precipitation to the Mars upper atmosphere under extreme solar wind conditions, *Geophys. Res. Lett.*, *40*, 1922–1927, doi:10.1002/grl.50415.
Fedorov, A., et al. (2006), Structure of the Martian wake, *Icarus*, *182*, 329–336, doi:10.1016/j.icarus.2005.09.021.
Fränz, M., E. Dubinin, E. Nielsen, J. Woch, S. Barabash, R. Lundin, and A. Fedorov (2010), Transterminator ion flow in the Martian ionosphere, *Planet. Space Sci.*, *58*, 1442–1454, doi:10.1016/j.pss.2010.06.009.
Harnett, E. M., and R. M. Winglee (2003), The influence of a mini-magnetopause on the magnetic pileup boundary at Mars, *Geophys. Res. Lett.*, *30*, 2074, doi:10.1029/2003GL017852.
Harnett, E. M., and R. M. Winglee (2006), Three-dimensional multifluid simulations of ionospheric loss at Mars from nominal solar wind conditions to magnetic cloud events, *J. Geophys. Res.*, *111*, A09213, doi:10.1029/2006JA011724.
Kallio, E., and H. Koskinen (1999), A test particle simulation of the motion of oxygen ions and the solar wind protons, *J. Geophys. Res.*, *104*, 557–579, doi:10.1029/1998JA900043.
Kallio, E., H. Koskinen, S. Barabash, C. M. C. Nairn, and K. Schwingenschuh (1995), Oxygen outflow in the Martian magnetotail, *Geophys. Res. Lett.*, *22*, 2449–2452, doi:10.1029/95GL02474.
Kallio, E., et al. (2006a), Ion escape from Mars: Comparison of a 3-D hybrid simulation with Mars Express IMA/ASPERA-3 measurements, *Icarus*, *182*, 350–359.
Kallio, E., et al. (2006b), Energisation of O^+ and O_2^+ ions at Mars: An analysis of a 3-D quasi-neutral hybrid model simulation, *Space Sci. Rev.*, *126*, 39–62.
Kallio, E., A. Fedorov, E. Budnik, S. Barabash, R. Jarvinen, and P. Janhunen (2008), On the properties of O^+ and O_2^+ ions in a hybrid model and in Mars Express IMA/ASPERA-3 data: A case study, *Planet. Space Sci.*, *56*, 1204–1213.
Ledvina, S. A., Y. Ma, and E. Kallio (2008), Modeling and simulating flowing plasmas and related phenomena, *Space Sci. Rev.*, *139*, 143–189.
Li, L., and Y. Zhang (2009), Model investigation of the influence of the crustal magnetic field on the oxygen ion distribution in the near Martian tail, *J. Geophys. Res.*, *114*, A06215, doi:10.1029/2008JA013850.
Liemohn, M. W., S. M. Curry, X. Fang, and Y. Ma (2013), Comparison of high-altitude production and ionospheric outflow contributions to O^+ loss at Mars, *J. Geophys. Res Space Physics*, *118*, 4093–4107, doi:10.1002/jgra.50388.
Luhmann, J. G., and J. U. Kozyra (1991), Dayside pickup oxygen ion precipitation at Venus and Mars: Spatial distributions, energy deposition and consequences, *J. Geophys. Res.*, *96*(A4), 5457–5467, doi:10.1029/90JA01753.
Luhmann, J. G., and K. Schwingenschuh (1990), A model of the energetic ion environment of Mars, *J. Geophys. Res.*, *95*, 939–945, doi:10.1029/JA095iA02p00939.
Lundin, R., et al. (1989), First results of the ionospheric plasma escape from Mars, *Nature*, *341*, 609–612, doi:10.1038/341609a0.
Lundin, R., et al. (2004), Solar wind-induced atmospheric erosion at Mars: First results from ASPREA-3 on Mars Express, *Science*, *305*, 1993–1936.
Ma, Y., A. F. Nagy, K. C. Hansen, D. L. De Zeeuw, and T. I. Gombosi (2002), Three- dimensional multispecies MHD studies of the solar wind interaction with Mars in the presence of crustal fields, *J. Geophys. Res.*, *107*, 1282, doi:10.1029/2002JA009293.
McKenna-Lawlor, S. M. P., V. Afonin, Y. Yeroshenko, E. Keppler, E. Kirsch, and K. Schwingenschuh (1993), First identification in energetic particles of characteristic plasma boundaries at Mars and an account of various energetic particle populations close to the planet, *Planet. Space Sci.*, *41*, 373.
Modolo, R., G. M. Chanteur, E. Dubinin, and A. P. Matthews (2005), Influence of the solar EUV flux on the Martian plasma environment, *Ann. Geophys.*, *23*, 433–444.
Najib, D., A. F. Nagy, G. Tóth, and Y. Ma (2011), Three-dimensional, multifluid, high spatial resolution mhd model studies of the solar wind interaction with mars, *J. Geophys. Res.*, *116*, A05204, doi:10.1029/2010JA016272.
Nilsson, H., N. J. T. Edberg, G. Stenberg, S. Barabash, M. Holmstrm, Y. Futaana, R. Lundin, and A. Fedorov (2011), Heavy ion escape from Mars, influence from solar wind conditions and crustal magnetic fields, *Icarus*, *215*(2), 475–484, doi:10.1016/j.icarus.2011.08.003.
Nilsson, H., G. Stenberg, S. Futaana, M. Holmstrom, S. Barabash, R. Lundin, N. Edberg, and A. Fedorov (2012), Ion distributions in the vicinity of Mars: Signatures of heating and acceleration processes, *Earth Planets Space*, *64*(2), 135–148, doi:10.5047/eps.2011.04.011.
Trotignon, J. G., E. Dubinin, R. Grard, S. Barabash, and R. Lundin (1996), Martian planetopause as seen by the plasma wave system onboard Phobos 2, *J. Geophys. Res.*, *96*(A11), 24,965–24,977, doi:10.1029/96JA01898.
Verigin, M. I., et al. (1991), Ions of planetary origin in the Martian magnetosphere (Phobos 2/TAUS experiment), *Plant. Space Sci.*, *39*, 131–137.
Vignes, D., et al. (2000), The solar wind interaction with Mars: Locations and shapes of the bow shock and the magnetic pile-up boundary from the observations of the MAG/ER experiment onboard Mars Global Surveyor, *Geophys. Res. Lett.*, *27*(1), 49–52, doi:10.1029/1999GL010703.
Wang, X. D., S. Barabash, Y. Futaana, A. Grigoriev, and P. Wurz (2013), Directionality and variability of energetic neutral hydrogen fluxes observed by Mars Express, *J. Geophys. Res. Space Physics*, *118*, 7635–7642, doi:10.1002/2013JA018876.
Yamauchi, M., et al. (2007), IMF direction derived from cycloid-like ion distributions observed by Mars Express, *Space Sci. Rev.*, *126*(1–4), 239–266, doi:10.1007/s11214-006-9090-1.